ARMY RESEARCH LABORATORY

Scanning Probe Investigation of Pitting Corrosion on Aluminum 5083 H131

by Joseph P. Labukas and Kenneth E. Strawhecker

ARL-TR-6925 May 2014

NOTICES

Disclaimers

The findings in this report are not to be construed as an official Department of the Army position unless so designated by other authorized documents.

Citation of manufacturer's or trade names does not constitute an official endorsement or approval of the use thereof.

Destroy this report when it is no longer needed. Do not return it to the originator.

Army Research Laboratory
Aberdeen Proving Ground, MD 21005-5069

ARL-TR-6925 **May 2014**

Scanning Probe Investigation of Pitting Corrosion on Aluminum 5083 H131

Joseph P. Labukas and Kenneth E. Strawhecker
Weapons and Materials Research Directorate, ARL

REPORT DOCUMENTATION PAGE	Form Approved OMB No. 0704-0188

1. REPORT DATE *(DD-MM-YYYY)*	2. REPORT TYPE	3. DATES COVERED (From - To)
May 2014	Final	2013–2014

4. TITLE AND SUBTITLE
Scanning Probe Investigation of Pitting Corrosion on Aluminum 5083 H131

5a. CONTRACT NUMBER

5b. GRANT NUMBER

5c. PROGRAM ELEMENT NUMBER

6. AUTHOR(S)
Joseph P. Labukas and Kenneth E. Strawhecker

5d. PROJECT NUMBER

5e. TASK NUMBER

5f. WORK UNIT NUMBER

7. PERFORMING ORGANIZATION NAME(S) AND ADDRESS(ES)
U.S. Army Research Laboratory
ATTN: RDRL-WMM-C
Aberdeen Proving Ground, MD 21005-5066

8. PERFORMING ORGANIZATION REPORT NUMBER
ARL-TR-6925

9. SPONSORING/MONITORING AGENCY NAME(S) AND ADDRESS(ES)

10. SPONSOR/MONITOR'S ACRONYM(S)

11. SPONSOR/MONITOR'S REPORT NUMBER(S)

12. DISTRIBUTION/AVAILABILITY STATEMENT
Approved for public release; distribution is unlimited.

13. SUPPLEMENTARY NOTES

14. ABSTRACT
An analytical approach to understanding the fundamental mechanisms of microscale corrosion has been developed. Aluminum alloy 5083 (H131 temper) was characterized before, during, and after corrosion in aqueous environments of varying ionic strength and pH. Morphological changes were observed both in situ and ex situ using atomic force microscopy. Compositional differences of alloy surfaces were mapped and identified using scanning Kelvin probe microscopy, scanning electron microscopy, and energy dispersive x-ray spectroscopy.

15. SUBJECT TERMS
corrosion, aluminum 5083, scanning probe, atomic force microscope, Kelvin probe

16. SECURITY CLASSIFICATION OF:			17. LIMITATION OF ABSTRACT	18. NUMBER OF PAGES	19a. NAME OF RESPONSIBLE PERSON
a. REPORT	b. ABSTRACT	c. THIS PAGE			Joseph P. Labukas
Unclassified	Unclassified	Unclassified	UU	26	19b. TELEPHONE NUMBER (*Include area code*) 410-306-2989

Contents

List of Figures

List of Tables

1. Introduction

Wrought aluminum (Al) alloys are used ubiquitously in the automotive, aerospace, and marine industries. The military uses several Al alloys of the 5000 series for a variety of vehicles, ships, and equipment because of the unique combination of physical properties (e.g., high strength, corrosion resistance, weldability, availability, and cost) of these alloys (*1*). In particular, Al alloy AA5083 (H131 temper) is used in armor applications and performs well in corrosive environments (*1*). However, the corrosion resistance of alloys in the 5000 series can be severely undermined when coupled galvanically to a more noble metal or when the alloy is exposed to temperatures at which sensitization occurs (*2–7*).

During sensitization of AA5083, magnesium (Mg) atoms migrate to grain boundaries where Al_3Mg_2, commonly referred to as the β phase, is formed (*2–4*). The process occurs in alloys of this series with greater than 3% (w/w) Mg concentration at temperatures as low as 50 °C (*2–4*). The β phase is more electrochemically active than the surrounding matrix in corrosive environments, and the rapid dissolution of this phase results in intergranular attack of the alloy (*2–7*). Sensitization has been reported to diminish the structural properties (i.e., strength and hardness) of the alloy (*8*).

Although intergranular corrosion is the most devastating to the mechanical properties of AA5083, pitting corrosion (*9, 10*) can also impact mechanical properties, finish, and adhesion of a coating. Understanding the mechanistic details of localized pitting corrosion involves the use of a variety of analytical techniques. Scanning probe techniques such as atomic force microscopy (AFM) (*11–13*) and scanning Kelvin probe microscopy (SKPM) (*14–16*) have been used with scanning electron microscopy (SEM) and energy dispersive x-ray spectroscopy (EDS) to probe corrosion of 2000- and 3000-series Al alloys (*15–19*). More specifically, SKPM and AFM were useful in establishing a linear relationship between the open circuit potential (OCP) and the Volta potential difference for several metals and the influence of the AFM tip on the corroding surface was addressed (*15–20*). Davoodi et al. (*21, 22*) have used scanning electrochemical microscopy in conjunction with in situ AFM, SKPM, EDS, and SEM to elucidate the role of intermetallic particles in the corrosion of 3000-series alloys. Intermetallic phases of AA5083 have been studied using AFM, SKPM, SEM, and EDS for AA5083 and typically iron (Fe)-rich phases are known to be local cathodes whereas silicon (Si)-containing precipitates act as anodes relative to the bulk (*23*, *24*).

Traditionally, accelerated corrosion has facilitated the assessment of corrosion phenomena and coating performance at the U.S. Army Research Laboratory (ARL). For example, the corrosion performance of AA5083 in the neutral salt fog exposure test, ASTM B117 (*25*), and the cyclic corrosion test, GM 9540P (*26*), are shown in figure 1. It is difficult to discern a difference in corrosion susceptibility of the substrates used in these studies. Furthermore, results are

qualitative in nature and rely tremendously on sample preparation and proper maintenance of the corrosion chambers. The results of these tests neither provide any chemical information relevant to corrosion susceptibility nor highlight corrosion initiation points at the microscale. Recent upgrades to the experimental and analytical capabilities at ARL provide the means for a more fundamental approach to corrosion research.

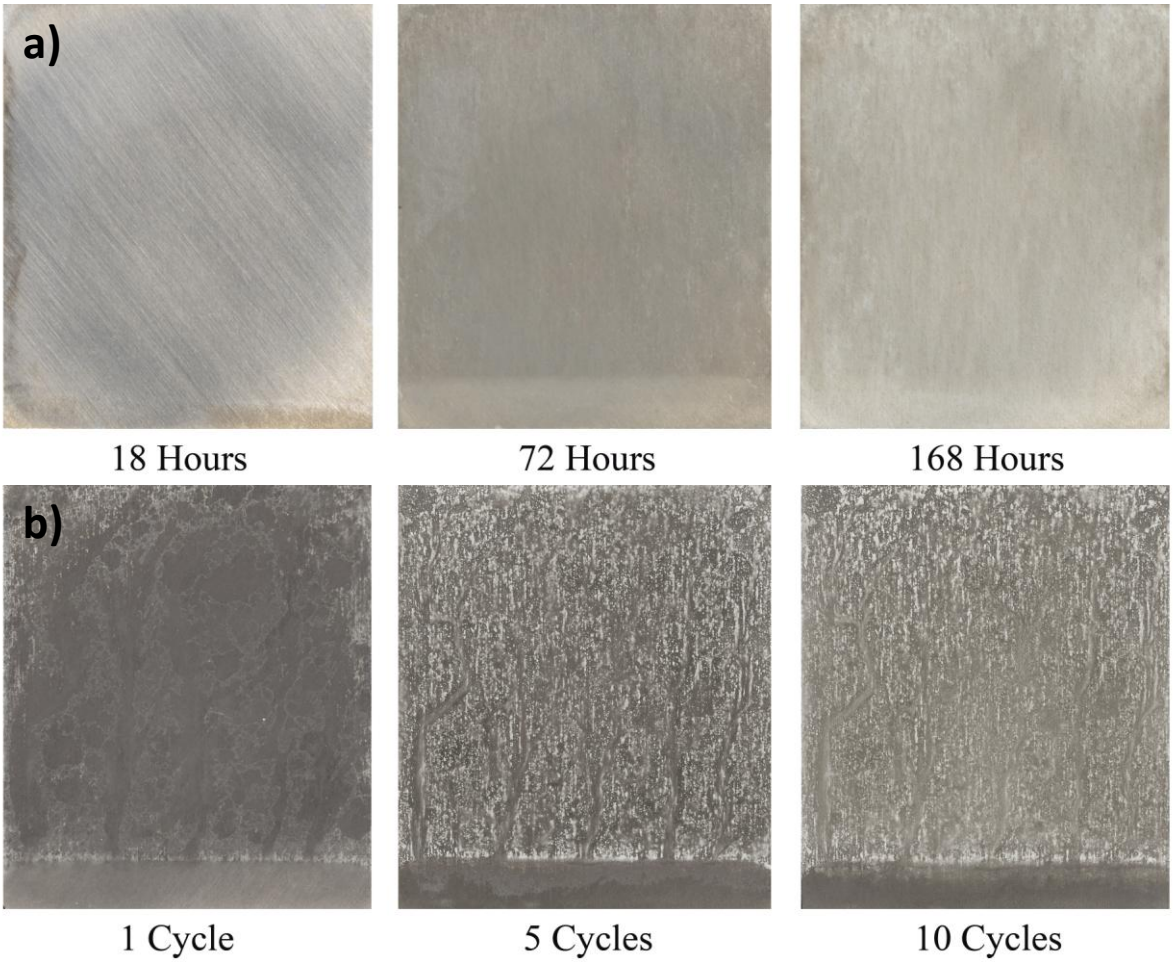

Figure 1. Accelerated corrosion of AA5083 during (a) ASTM B117 and (b) GM 9540P testing.

To establish our proficiency in using these techniques, we focused on studying the well-known pitting corrosion of AA5083 using in situ AFM, wherein we continuously scan the sample surface immersed in a variety of corrosive environments. We investigated topographic features and surface potential before and after corrosion with AFM and SKPM to highlight the role of secondary phases. Localized chemical identification was obtained using EDS before and after corrosion. Potentiodynamic polarization of samples in several environments was used to understand the effects of pH and concentration on electrochemical behavior of unsensitized AA5083.

2. Experimental

2.1 Materials

Sodium chloride (NaCl) (99%, VWR International), silver wire (>99.99%, Aldrich), hydrochloric acid (HCl) (37%, Sigma-Aldrich), potassium hydroxide (85%, EMD Chemicals) and ethanol (200 proof, Warner Graham Co.) were used as received from the manufacturers. Deionized (DI) water, purified to a resistivity of 18.2 MΩ cm (Millipore Corp.), was used for all of the solutions.

2.2 Sample Preparation

AA5083 H131 (approximately 1 × 1 × 0.2 cm) was ground with successively higher-grit silicon carbide paper to 1200, then polished in a stepwise fashion from 9 to 3 to 1 μm using aqueous diamond suspensions (MetaDi). The final size of AA5083 substrates for scanning probe experiments was approximately 1 × 1 × 0.2 cm. Immediately after polishing, samples were rinsed thoroughly with ethanol, DI water, sonicated in ethanol for 30 s, rinsed with ethanol, and blown dry with a stream of nitrogen. Samples that had been stored for more than 24 h prior to use were sonicated in ethanol for 30 s, rinsed with ethanol, and blown dry with a stream of nitrogen.

2.3 Atomic Force Microscopy/Scanning Kelvin Probe Microscopy

An Asylum MFP-3D atomic force microscope was used to study the topography and map the potential across a sample surface. For topography in air, scans were collected in tapping mode using a doped diamond-coated etched-silicon probe (DDESP) tip (Bruker Biosciences Corp.). This conductive tip was used to simultaneously collect scanning Kelvin probe data. Using the SKPM routine of the MFP-3D software, a topographic scan is collected on one line of the image, the tip is raised above the sample surface to a constant height of 50 nm or less, and the probe traces the same path from which the topographic features were generated. It is during this second trace path that Kelvin probe data is collected.

In situ AFM was performed using an electrochemical cell provided by the manufacturer. A picture of the cell is seen in figure 2. The surface area of the working electrode (AA5083) is approximately 1 cm^2. Contact mode AFM was used so that adsorbates on the tip and the presence of corrosion products on the surface do not affect the clarity of the topographical changes in the scan region. The electrolyte volume was replaced once per day for scans that lasted more than 24 h.

Figure 2. Electrochemical cell for in situ AFM measurements.

2.4 Potentiodynamic Polarization

Using a flat cell (EG&G) consisting of AA5083 as the working electrode, platinum-coated mesh (Intrepid Industries) as the counter electrode, and a saturated calomel electrode (Gamry) as the reference electrode, polarization curves of AA5083 were collected using a potentiostat (Gamry Reference 600). Potentiodynamic polarization was done under ambient laboratory conditions from –0.3 V of the OCP to 1.0 V more than OCP at a scan rate of 1 mV/s.

2.5 Scanning Electron Microscopy/Energy Dispersive X-ray Spectroscopy

A Hitachi S4700 SEM was used to image surfaces before and after corrosion. Energy dispersive spectroscopy was used to obtain chemical composition at the metal surface.

3. Results and Discussion

3.1 Microstructure and Local Elemental Composition

Scanning electron microscopy was used to identify the morphology of the native Al surface after polishing. An image of a precipitate particle that is representative of those most commonly found in AA5083 H131 is shown in figure 3. Cracks within the particle are a result of the rolling that this alloy plate undergoes during processing steps that tailor the mechanical properties. Energy dispersive spectroscopy was used to identify elemental differences between spots 1 and 2 in figure 3. Elemental analysis (table 1) of the precipitate (figure 3, spot 1) shows the presence of manganese (Mn), Fe, and chromium (Cr) in addition to bulk Al and Mg solid solution (figure 3, spot 2). Although smaller particles can be seen in the SEM image, differences in chemical composition of small and large particles were not discernible by EDS. In fact, similar compositions were observed for all other precipitates in this report. Literature values of the elemental composition limits of Al, Mg, Mn, Fe, and Cr, and are also shown in table 1.

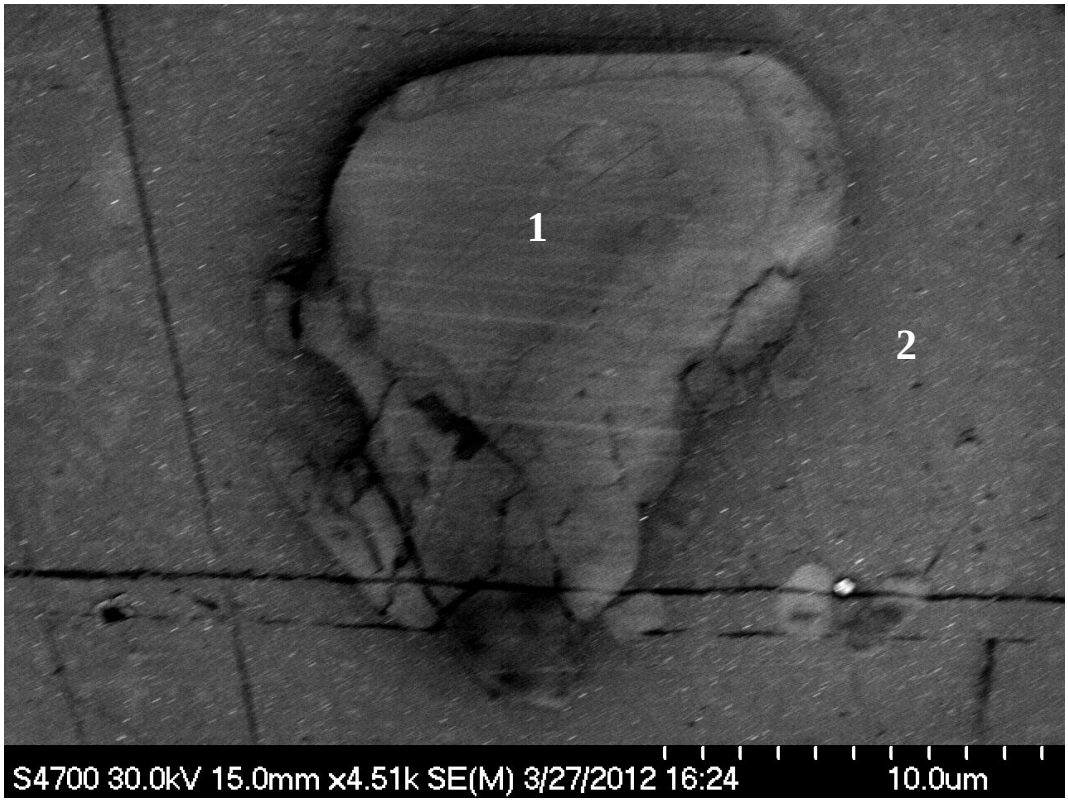

Figure 3. SEM Image of precipitate found in AA5083 H131.

Table 1. Chemical composition of two regions on AA5083 measured using EDS.

Element	**Atomic (%)**		
	Spot 1	**Spot 2**	**Literature (*27*)**
Al	91.07	93.86	93.45–95.91
Mg	5.39	5.65	4.0–4.9
Mn	1.60	0.49	0.04–1.0
Fe	1.74	0.00	0.00–0.40 max
Cr	0.20	0.00	0.05–0.25

3.2 In Situ Atomic Force Microscopy and Scanning Kelvin Probe Microscopy

A unique advantage to studying corrosion with AFM is that pit growth can be measured accurately around individual precipitates. Topographic and potential differences across the surface of AA5083 H131, using tapping-mode AFM and constant-height-mode SKPM, respectively, revealed precipitates in the bulk matrix similar in size and shape to those found using SEM. The topographic map shows these precipitates as raised spots that are lighter in color than the surrounding matrix (figure 4a). These precipitate particles are raised because the precipitate eroded at a slower rate than the bulk during the mechanical polishing step due to a difference in hardness. Figure 4b shows the Volta potential map of the same area measured with

the scanning Kelvin probe; however, in this mode of operation, the hard precipitates show up as dark spots (lower potential difference relative to the AFM tip). These differences in intensity across the Volta potential map represent relative potential difference between the diamond coating on the AFM tip and the local surface potential. Dark spots indicate small Volta potential differences whereas light spots represent large differences (i.e., deflection of the cantilever above hard precipitates is smaller than the deflection measured above the bulk matrix). These differences, which are measured in air, have been shown to be linearly related to the OCP of materials in solution (*15*, *16*, *19*). This relationship between Volta potential and OCP can be used as a predictive tool for identifying where localized dissolution may occur on a sample surface and for understanding the electrochemical mechanism that drives corrosion (*15*, *16*, *19*).

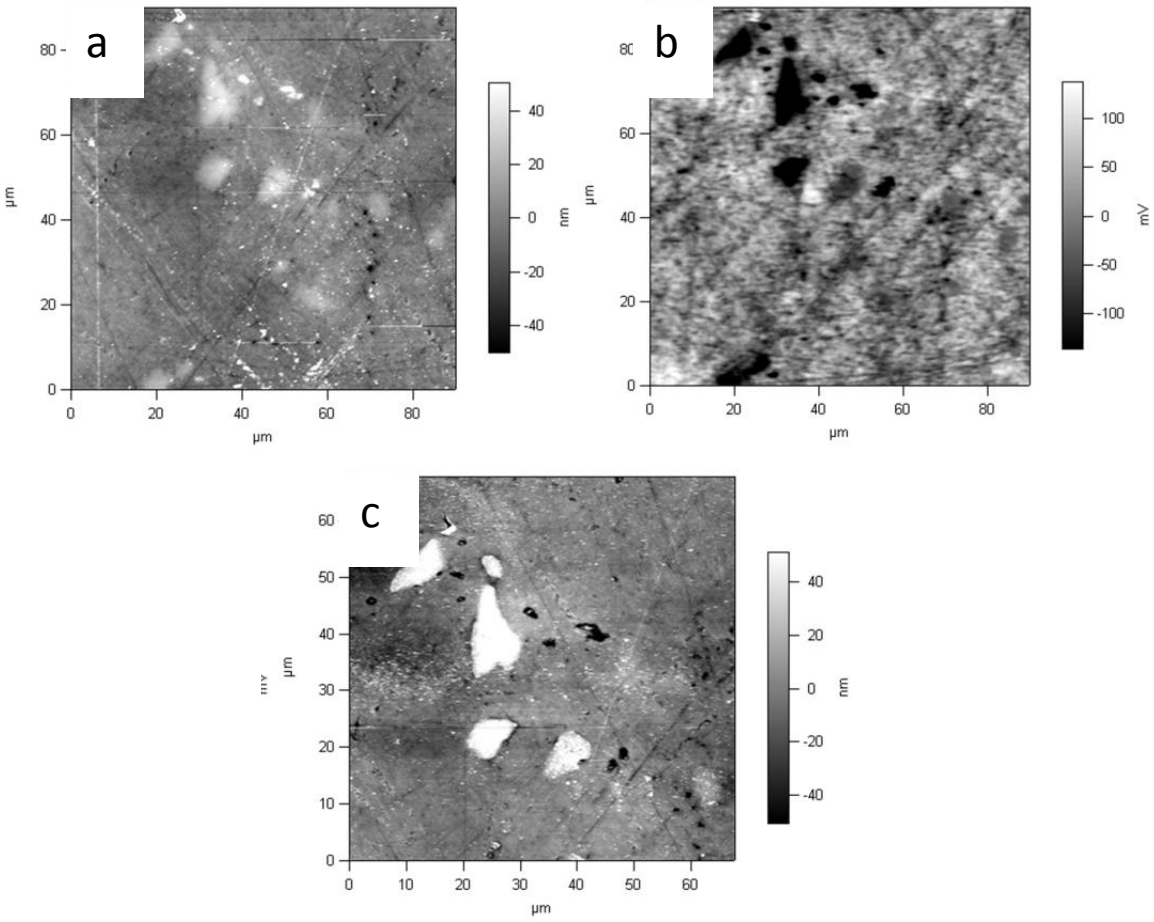

Figure 4. Scanning probe images of an AA5083 H131 surface showing (a) topography in air, (b) Volta potential in air, and (c) topography in 0.1-M NaCl solution.

Based on the SKPM observations, we expected to see the bulk Al matrix dissolve around the intermetallic particles of AA5083. Figure 4c is an AFM image showing topographic features of the AA5083 surface while immersed in 0.1-M NaCl (aqueous). This was the first image collected after immersion. Immediate pit formation was observed around smaller particles that are more noble than the bulk based on Volta potential differences measured with SKPM. Other evidence that the nobility of these particles is greater than the bulk Al phase is the chemical composition determined by EDS, which shows the presence of Mn and Fe. These small particles seen in the dry topographic scan and the SKPM images may have been undercut and fallen out or dissolved during the initial stages of corrosion.

A sequence of AFM images of AA5083 in the dry state, the wetted state immediately after exposure to 100-mM NaCl solution, and after approximately 200 min of NaCl (aqueous) exposure (figure 5a–c, respectively) reveals continuous pit growth around cathodic particles. Small particles similar to those within the red circles shown in figure 5 are dislocated rapidly upon immersion into NaCl solution, and a pit is subsequently formed. Dislocation of the particle may have been facilitated by the AFM tip, formation of corrosion products, or dissolution of the particle during the time it took to capture the AFM image. This type of pitting behavior has been previously reported for copper-containing Al 2024-T3 (*28*). Similarly, pitting corrosion around larger precipitates (shown in blue rectangles, figure 5) proceeds outward from the precipitate into the bulk as expected based on the relative nobility of the particle. At this time it is unclear what the driving force is that facilitates corrosion around one particle and not another; however, local differences in oxide-layer thickness, defects incorporated due to polishing, or changes in local solution composition may play a role in determining the location of initial dissolution. Figure 6 shows the cross-sectional changes in topography across the colored lines drawn through the particles located within the blue rectangle of figure 5 measured over approximately 3 h.

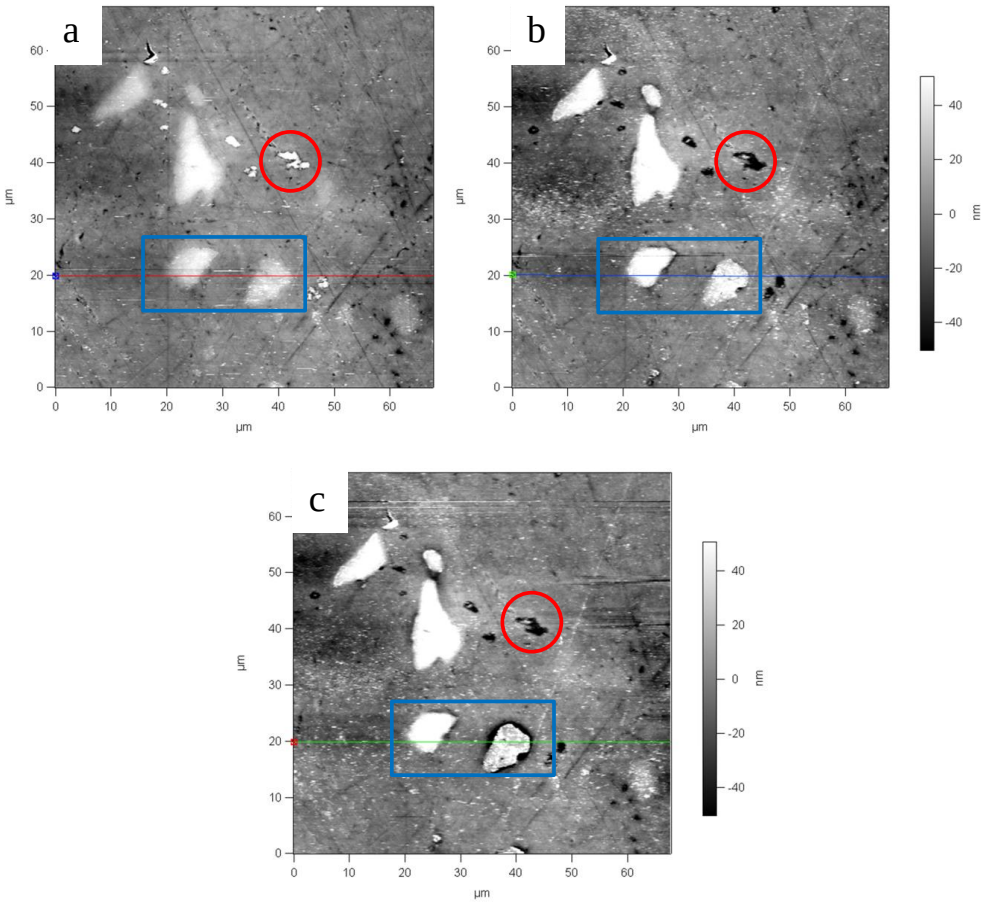

Figure 5. AFM images of AA5083 in (a) the dry state, (b) the wetted state immediately after exposure to 100-mM NaCl solution, and (c) after approximately 200 min of NaCl (aqueous).

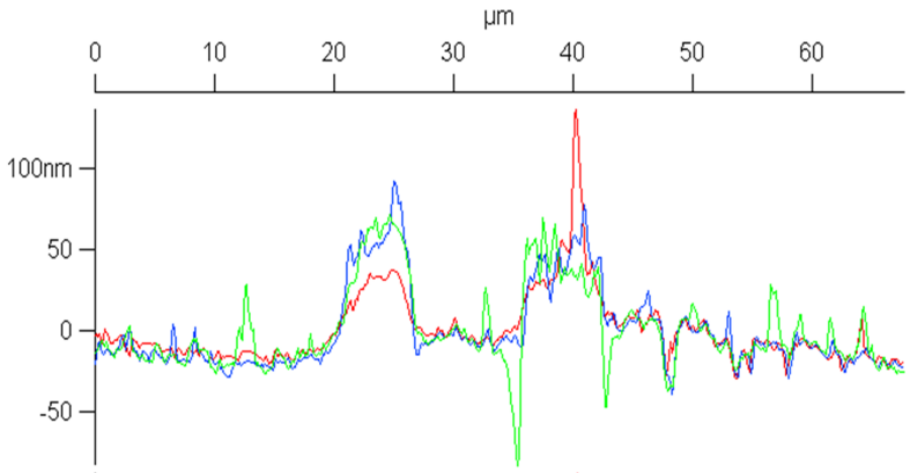

Figure 6. Depth profile across a region of AA5083 (shown in figure 5) while corroding (red = dry; blue = initial min in 100-mM NaCl solution; green = approximately 200 min in 100-mM NaCl solution).

In situ corrosion experiments on AA5083 using the AFM was also done in 1- and 10-mM NaCl (aqueous) solutions. The progression of bulk dissolution in the 1-mM solution is shown in figure 7. Again, corrosion initiates at the edge of an intermetallic particle and progresses around the particle into the bulk. In the particular example shown in figure 7, the boundaries of the precipitate are not as clear until later in the corrosion of the particle shown in the white circle. The lack of contrast (i.e., topography) may be due of variations in sample polishing conditions that result in smaller differences in height between bulk Al matrix and the precipitate. A comparison of the rate of maximum pit depth with respect to electrolyte concentration is shown in figure 8. As expected, the sample immersed in 100-mM NaCl corroded much faster than the sample immersed in 1-mM NaCl.

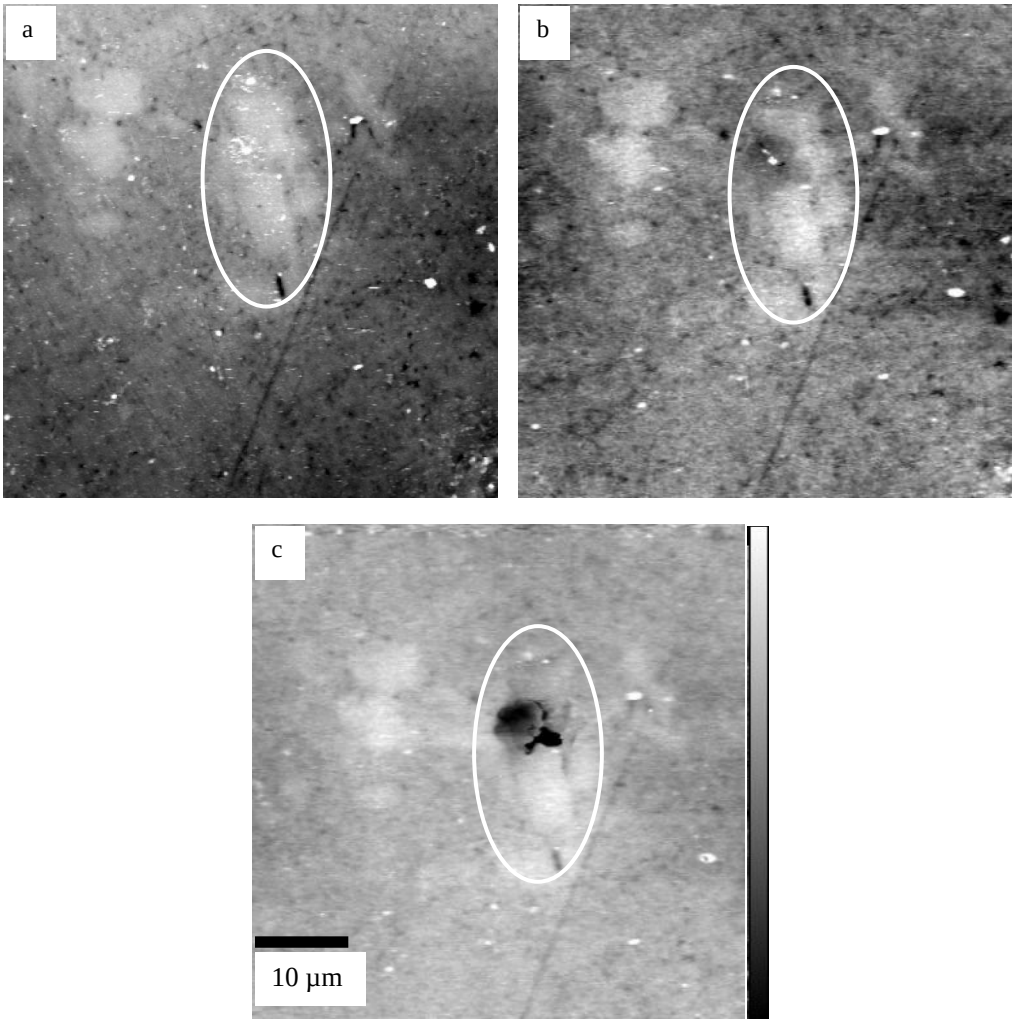

Figure 7. In situ corrosion of AA5083 in 1-mM NaCl.

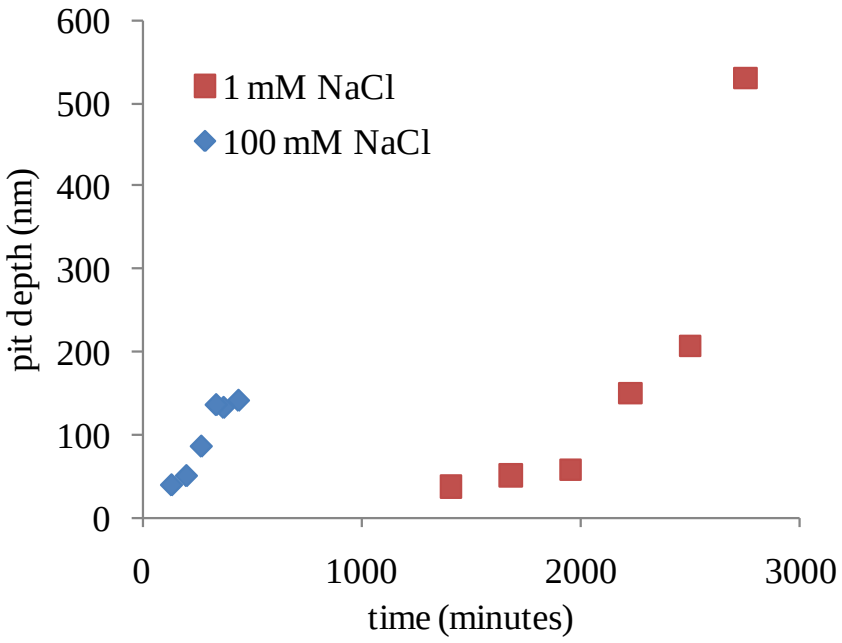

Figure 8. Pit depth with respect to time for two concentrations of NaCl electrolyte.

Careful consideration should be taken when calculating pit volume with scanning probe techniques. For instance, AFM is not able to measure material being displaced beneath a particle. Similarly, the aspect ratio of a pit may lead to inaccurate measurement of pit dimensions due to limitations of the instrument and the influence of the wall of the pit on the tip travel (i.e., piezo travel distance, tip shape, and aspect ratio). Other important considerations for using in situ AFM for corrosion have been reported throughout the literature and have been verified in our experiments. First, the effect of the tip on the substrate can induce corrosion. In our studies, pit growth around particles was seen in the area that the AFM probe was being rastered but not in areas outside of the scan region. Also, the area over which the probe is being rastered is affected by the probe interaction with the surface, as seen by the rectangular area in figure 9, which is lower than the rest of the representative 5000-series Al matrix. The erosion in this area is likely to be a combination of (1) corrosion products being swept toward the edges of the scan area and (2) the tip scratching through the protective native oxide layer protecting the surface.

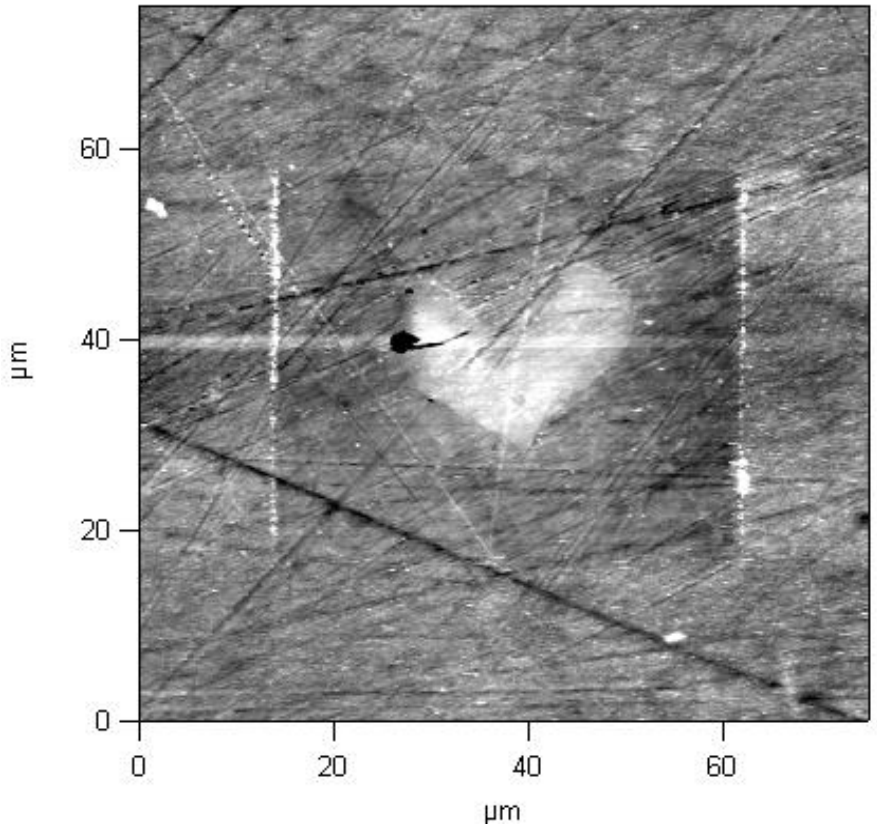

Figure 9. Surface modification resulting from tip-sample interaction with a 5000-series Al alloy during in situ AFM scanning

3.3 Electrochemical Measurements

Samples of AA5083 H131 were polarized in different concentrations of NaCl to observe the effect of concentration on the corrosion potential (E_{corr}) and corrosion current (I_{corr}) (figure 10). Chloride ion concentration does not significantly change the corrosion potential of AA5083 over the range of concentrations used in this study. As chloride ion in solution is increased, however, dissolution of the passive oxide layer on the Al alloy is increased and corrosion rate is thereby increased. Further investigation into the mechanism of oxide layer breakdown in a variety of environments may aide in designing more robust oxide surfaces for corrosion protection.

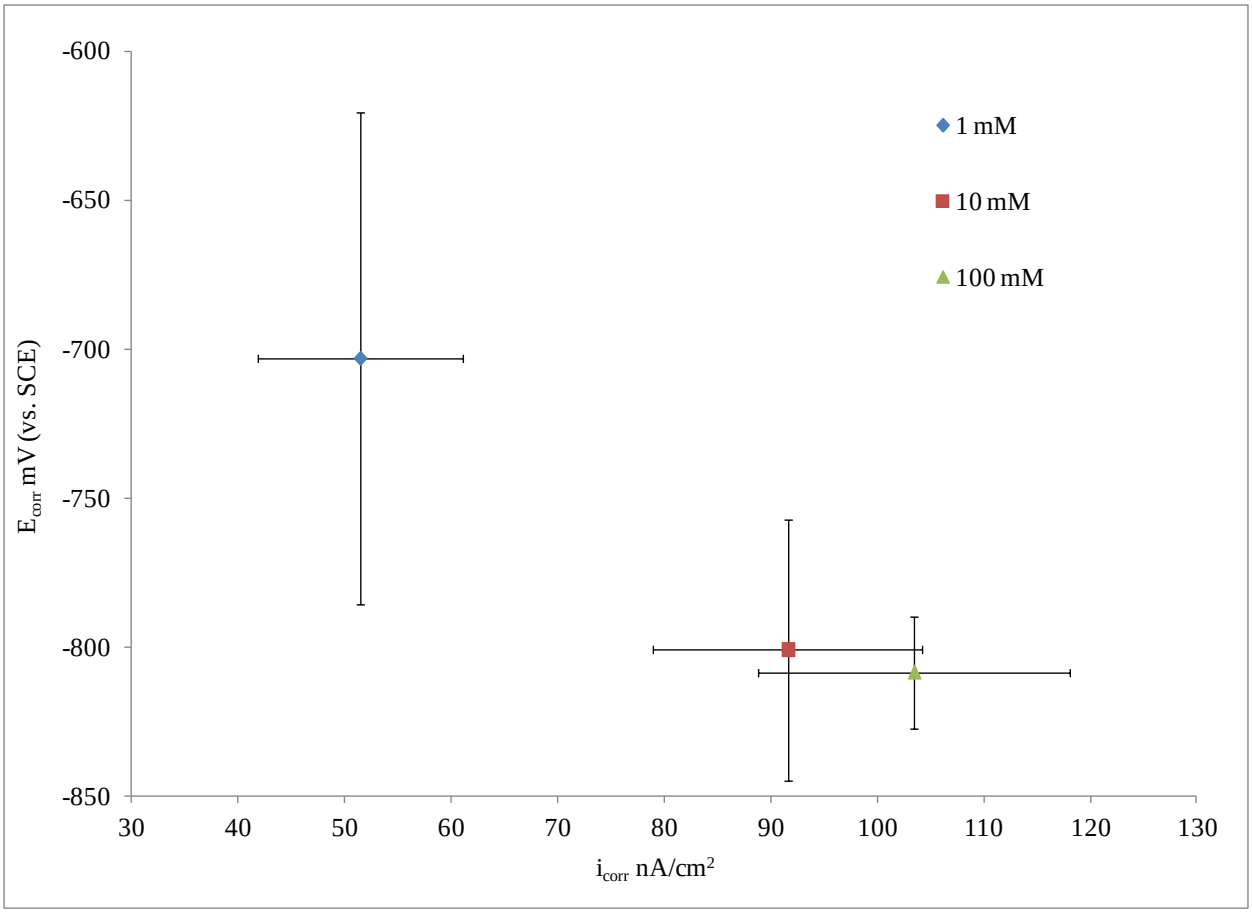

Figure 10. A plot of OCP vs. corrosion current showing the effect of concentration on corrosion parameters.

4. Conclusions

Recent modernizations of the experimental and analytical capabilities at ARL provide the means for fundamental corrosion research. Our approach to proficiency in using these techniques focused on studying the well-known pitting corrosion of AA5083 using in situ AFM, wherein we continuously scan the sample surface immersed in a variety of corrosive environments. We investigated topographic features and surface potential before and after corrosion with AFM and SKPM to highlight the role of secondary phases. Secondary phases were found to be more noble than the bulk and served as initiation points for pitting corrosion on the surface of AA5083 H131. Localized chemical identification was obtained using EDS before and after corrosion. It was found that the precipitates were rich in Fe and Mn, which contributed to the ennoblement of their potential. Potentiodynamic polarization of samples in several environments was used to understand the effects of NaCl electrolyte concentration on electrochemical behavior of unsensitized AA5083. Increasing the electrolyte concentration increased the rate of dissolution of the bulk phase of the alloy.

5. References

1. Placzankis, B. E. *General Corrosion Resistance Comparisons of Medium- and High-Strength Aluminum Alloys for DOD Systems Using Laboratory-Based Accelerated Corrosion Methods;* ARL-TR-4937; U.S. Army Research Laboratory: Aberdeen Proving Ground, MD, September 2009.

2. Goswami, R.; Spanos, G.; Pao, P. S.; Holtz, R. L. Precipitation Behavior of the Beta Phase in Al5083. *Materials Science and Engineering A-Structural Materials Properties Microstructure and Processing* **2010,** *527* (4), 1089–1095.

3. Dix, H.; Anderson, W. A.; Shumaker, M. B. Influence of Service Temperature on the Resistance of Wrought Aluminum-Magnesium Alloys to Corrosion. *Corrosion* **1959,** *15* (1), 55–62.

4. Searles, J. L.; Guoma, P. I.; Buchheit. R. G. Stress Corrosion Cracking of Sensitized AA5083 (Al-4.5Mg-1.0Mn). *Metallurgical and Materials Transactions A* **2001,** *32A,* 2859–2867.

5. Lim, M. L.; Jain, S.; Kelly, R. G.; Scully, J. R. Intergranular Corrosion Penetration in AA5083 (UNS# A95083) as a Function of Electrochemical and Metallurgical Conditions. *ECS Transactions* **2012,** *41* (25), 177–191.

6. Buchheit, R. G.; Boger, R. K.; Carroll, M. C.; Leard, R. M.; Pagila, C.; Searles, J. L. The Electrochemistry of Intermetallic Particles and Localized Corrosion in Al Alloys. *JOM* **2001,** *53,* 29–33, 36.

7. Buchheit. R. G. A Compilation of Corrosion Potentials Reported for Intermetallic Phases in Aluminum Alloys. *J. Electrochem. Soc*. **1995,** *142* (11), 3994–3996.

8. Oguocha, I. N. A.; Adigun, O. J.; Yannacopoulos. S. Effect of Sensitization Heat Treatment on Properties of Al-Mg alloy AA5083-H116. *Journal of Materials Science* **2008,** *43,* 4208–4214.

9. Gupta, R. K.; Sukiman, N. L.; Cavanaugh, M. K.; Hinton, B. R. W.; Hutchinson, C. R.; Birbilis, N. Metastable Pitting Characteristics of Aluminum Alloys Measured Using Current Transients During Potentiostatic Polarization. *Electrochemica Acta* **2012,** *66,* 245–254.

10. Dolic, N.; Malina, J.; Begic Hadzipasic, A. Pit Nucleation on As-Cast Aluminum Alloy AW-5083 in 0.01M NaCl. *Journal of Mining and Metallurgy* **2011,** *47* (1) B, 79–87.

11. Birbilis, N.; Meyer, K.; Muddle, B. C.; Lynch, S. P. In Situ Measurement of Corrosion at the Nanoscale. *Corrosion Science* **2009,** *51,* 1569–1572.

12. Martin, T.; Hebert, K. R. Atomic Force Microscopy Study of Anodic Etching of Aluminum: Etching Morphology Development and Caustic Pretreatment. *Journal of the Electrochemical Society* **2001,** *148* (2), B101–B109.

13. Rynders, R. M.; Paik, C.-H.; Ke, R.; Alkire, R. C. Use of In Situ Atomic Force Microscopy to Image Corrosion at Inclusions. *J. Electrochem Soc*. **1994,** *141* (6), 1439–1445.

14. Yee, S.; Oriani, R. A.; Stratmann, M. Application of a Kelvin Microprobe to the Corrosion in Humid Atmospheres. *J. Electrochem Soc*. **1991,** *138* (1), 55–61.

15. Guillaumin, V.; Schmutz, P.; Frankel, G. S. Characterization of Corrosion Interfaces by the Scanning Kelvin Probe Force Microscopy Technique. *J. Electrochem Soc*. **2001,** *148* (5), B163K–B173K.

16. Schmutz, P.; Frankel, G. S. Characterization of AA2024-T3 by Scanning Kelvin Probe Force Microscopy. *J. Electrochem. Soc*. **1998,** *145* (7), 2285–2295.

17. DeLuccia, K. J.; Josefowicz, J. Y.; Laird, C.; Farrington, G. C. In Situ Atomic Force Microscopy Observations of the Corrosion Behavior of Aluminum-Copper Alloys. *J. Electrochem Soc*. **1996,** *143* (8), 2471–2481.

18. Leblanc, P.; Frankel. G. S. A Study of Corrosion and Pitting Initiation of AA2024-T3 Using Atomic Force Microscopy. *Journal of the Elelctochemical Society* **2002,** *149* (6), B239–B247.

19. Schmutz, P.; Frankel, G. S. Corrosion Study of AA2024-T3 by Scanning Kelvin Probe Force Microscopy and In Situ Atomic Force Microscopy Scratching. *J. Electrochem. Soc.* **1998,** *145* (7), 2295–2306.

20. Chen, L.; Guay, D. Selected Dissolution of Aluminum Initiated by Atomic Force Microscope Tip-Surface Interaction. *J. Electrochem. Soc*. **1994,** *141* (4), L43–L45.

21. Davoodi, A.; Pan, J.; Leygraf, C.; Norgren, S. Integrated AFM and SECM for In Situ Studies of Localized Corrosion of Al Alloys. *Electrochemica Acta* **2007,** *52,* 7697–7705.

22. Davoodi, A.; Pan, J.; Leygraf, C.; Norgren, S. Multianalytical and In Situ Studies of Localized Corrosion of EN AW-3003 Alloy: Influence of Intermetallic Particles. *J. Electrochem. Soc*. **2008,** *155* (4), C138–C146.

23. Yasakau, K. A.; Zheludkevich, M. L.; Lamaka, S. V.; Ferreira, M. G. S. Role of Intermetallic Phases in Localized Corrosion of AA5083. *Electrochemica Acta* **2007,** *52,* 7651–7659.

24. Aballe, A.; Bethencourt, M.; Botane, F. J.; Cano, M. J.; Marcos, M. Localized Alkaline Corrosion of Alloy AA5083 in Neutral 3.5% NaCl Solution. *Corrosion Science* **2001,** *43,* 1657–1674.

25. ASTM B117-90. Standard Method of Salt Spray (Fog) Testing. *Annu. Book ASTM Stand.* **1990**.

26. GM 9540P. *Accelerated Corrosion Test*. General Motors Engineering Standards, 1997.

27. Showalter, D. D.; Placzankis, B. E.; Burkins, M. S. *Ballistic Performance Testing of Aluminum Alloy 5059-H131 and 5059-H136 for Armor Applications;* ARL-TR-4427; U.S. Army Research Laboratory: Aberdeen Proving Ground, MD, May 2007.

28. Buchheit, R. G.; Grant, R. P.; Hlava, P. F.; Mckenzie, B.; Zender, G. L. Local Dissolution Phenomena Associated With S Phase (Al2CuMg) Particles in Aluminum Alloy 2024-T3. *J. Electrochem. Soc*. **1997,** *144* (8), 2621–2628.

1 DEFENSE TECHNICAL
(PDF) INFORMATION CTR
DTIC OCA

2 DIRECTOR
(PDF) US ARMY RESEARCH LAB
RDRL CIO LL
IMAL HRA MAIL & RECORDS MGMT

1 GOVT PRINTG OFC
(PDF) A MALHOTRA

3 DIR USARL
(PDF) RDRL WMM C
J LABUKAS
B PLACZANKIS
RDRL WMM G
K STRAWHECKER